

Proton Acceleration with High-Intensity Ultrahigh-Contrast Laser Pulses

T. Ceccotti,¹ A. Lévy,¹ H. Popescu,¹ F. Réau,¹ P. D'Oliveira,¹ P. Monot,¹ J. P. Geindre,² E. Lefebvre,³ and Ph. Martin¹

¹*Service des Photons, Atomes et Molécules, Commissariat à l'Energie Atomique, DSM/DRECAM, CEN Saclay, 91191 Gif sur Yvette, France*

²*LULI, UMR7605, CNRS-CEA-Ecole Polytechnique-Paris 6, 91128 Palaiseau, France*

³*Département de Physique Théorique et Appliquée, CEA/DAM Ile-de-France, BP 12, 91680 Bruyères-le-Châtel, France*

(Received 9 March 2007; published 31 October 2007)

We report on simultaneous measurements of backward- and forward-accelerated protons spectra when an ultrahigh intensity ($\sim 5 \times 10^{18}$ W/cm²), ultrahigh contrast ($>10^{10}$) laser pulse interacts with foils of thickness ranging from 0.08 to 105 μ m. Under such conditions, free of preplasma originating from ionization of the laser-irradiated surface, we show that the maximum proton energies are proportional to the p component of the laser electric field only and not to the ponderomotive force and that the characteristics of the proton beams originating from both target sides are almost identical. All these points have been corroborated by extensive 1D and 2D particle-in-cell simulations showing a very good agreement with the experimental data.

DOI: [10.1103/PhysRevLett.99.185002](https://doi.org/10.1103/PhysRevLett.99.185002)

PACS numbers: 52.38.Kd, 52.50.Jm, 52.70.Nc

The recent observations of intense energetic proton beams generated by interaction of high intensity ($\geq 10^{18}$ W/cm²) sub picosecond lasers with solid targets [1–3] have opened a new exciting field of research. These proton bunches allow for a better understanding of the underlying laser-solid interaction at very high intensities and are also considered for many practical purposes, such as high resolution probing of electric fields in plasmas [4], induction of nuclear phenomena [5], and fast ignition applications [6]. Up to now, most published works deal with protons emitted in the forward laser direction (FWD in the following) accelerated normally to the surface of the target, from the side opposite to laser irradiation. They generally exhibit a high laminarity, a low divergence ($<20^\circ$, decreasing with proton energy), and the estimated duration at the source lies in the picosecond range [7,8]. Protons originating from the laser-irradiated surface and accelerated in the backward direction (BWD in the following), are usually found much less energetic [9,10] and of less interest as a diagnostic or application tool. The admitted scenario for FWD proton acceleration involves three consecutive steps. First, the laser prepulse creates a thin plasma layer at the surface of the foil. Then, the intense part of the pulse interacting with this thin layer accelerates electrons toward the foil, essentially by the ponderomotive force. Finally, the electron beam reaches the rear surface and creates a strong electrostatic field which first ionizes and then accelerates protons and ions to high energies. This scenario, called Target Normal Sheath Acceleration (TNSA) [11] has been confirmed by several experiments [12]. Nevertheless, the influence of specific experimental conditions, for instance the laser contrast [13], on the electron acceleration toward the back of the target, and consequently on FWD and BWD emission characteristics, is not yet completely evident.

This Letter reports a study of proton acceleration using thin Mylar foils of different thickness as targets, under low

(10^6) and ultrahigh (10^{10}) laser contrast conditions (respectively “LC” and “HC” in the following). We performed simultaneous single shot measurements of proton emission behind the target in the laser direction (FWD) and in front of the target, opposite to laser direction (BWD). For both emission directions, the influence of the laser beam polarization on proton maximum energies is reported. We used 1D and 2D Particle-In-Cell (PIC) simulations to interpret our experimental data. Numerical results are in good agreement with collected data, pointing out both that increased electron confinement in the thinnest targets enhances the maximum proton energy and the dependence from the laser polarization.

The experiment has been performed at the Saclay Laser Interaction Center Facility, using the UHI10 laser which delivers 10 TW ultrashort pulses (65 fs) at 10 Hz repetition rate. This Ti-Sapphire laser is based on the standard chirped-pulse-amplification (CPA) technique and operates at a central wavelength of 790 nm. The intrinsic 10^6 contrast of the beam is raised to 10^{10} thanks to a “double plasma mirror” [14,15]. Under HC conditions, the spatial focal spot qualities are preserved while the laser energy is reduced by a factor of 2.

The laser beam was focused to a spot size of 8 μ m (FWHM) using an off-axis $f = 300$ mm parabola, under a 45° incidence angle and p polarization, on thin Mylar foils with thickness varying between 0.08 and 105 μ m. Maximum peak intensities close to 5×10^{18} W/cm² (HC) and 10^{19} W/cm² (LC) were reached. Proton spectra were recorded using two similar Thomson parabola spectrometers placed normally to the target surfaces at distances of 240 mm (BWD) and 600 mm (FWD). The entrance pin-hole diameter were respectively 100 μ m and 200 μ m. Once dispersed by the magnetic and electric fields of the spectrometer, protons and ions were detected by a two stage 40 mm diameter micro channel plate (MCP) coupled to a phosphor screen. This latter was imaged onto a 12 bit

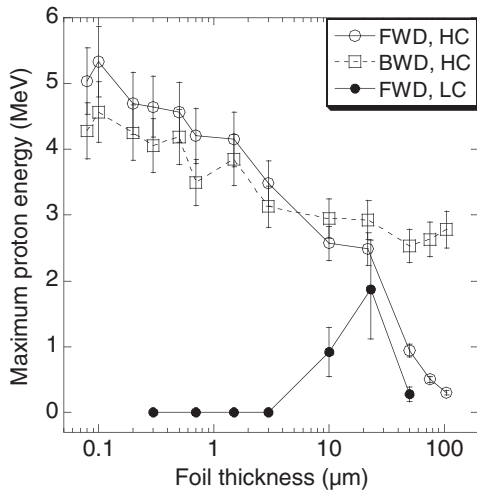


FIG. 1. Variation of maximum detectable proton energy as a function of target thickness. The FWD and BWD emissions for a laser contrast of 10^{10} (10^6) and intensity of 5×10^{18} W/cm 2 (10^{19} W/cm 2) are represented, respectively, by open (solid) circles and squares. Lines are a guide for the eye.

CCD camera and ion traces analyzed using simulated ion parabolas obtained through the commercial code SIMION. The MCP efficiency for proton energies in our range of interest was assumed linear [16,17].

We present in Fig. 1 the measurements of maximum detectable proton energies for different target thicknesses and laser contrast. Each point represents an average on at least three shots. Error bars correspond to the average standard deviation we found for three different test target thicknesses, repeating the same measure over around 30 shots. Besides protons, also important quantities of high-energy ion beams (essentially C^{n+}) have been detected from both surfaces of the targets. The emission properties of these ions will be the subject of a future communication to be published elsewhere.

In the case of LC data, we did not detect any ion in the BWD direction. As the pedestal-produced plasma strongly increases the ion beam divergence, we expect the signal to fall below the MCP sensibility threshold. As expected [18], FWD emission was characterized by the presence of an optimal value for the target thickness. The optimal thickness for Mylar targets was around $20 \mu\text{m}$ and the related maximum energy around 1.8 MeV in good agreement with previous measurements, performed under similar conditions [19,20]. The situation is drastically different for HC shots. For target thicknesses larger than $20 \mu\text{m}$, the BWD beam energies remain constant about 2.75 MeV whereas FWD energies rapidly decrease, exhibiting the same behavior as in the LC case. The electron transverse spreading seems then not to be affected by the pulse contrast. For foils thinner than $20 \mu\text{m}$, we observe that decreasing the target thickness down to 80 nm , BWD and FWD energies increase showing an identical behavior. The maximum energy, about 5 MeV , was obtained for a thickness of $0.1 \mu\text{m}$. The laser beam pedestal fluence being lower

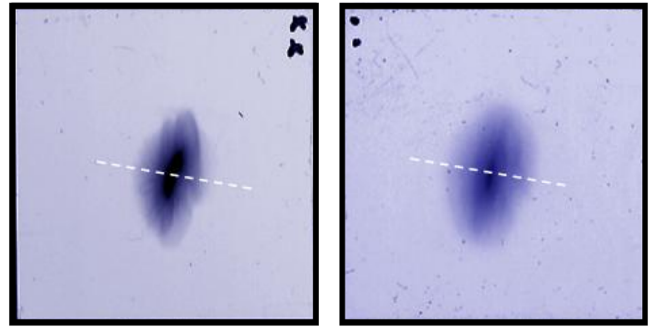


FIG. 2 (color online). Radiochromic films profiles in the FWD (left) and BWD (right) direction for the same shot. The estimated divergence along the dashed lines is around 4.5° for both proton beams.

than the target damage threshold, the irradiated and rear sides of the target are both substantially planar at the arrival of the main pulse. We can therefore suppose that protons are accelerated in both directions by practically the same planar charge separation. As a consequence, efficient TNSA is possible also for the front surface protons which must show the same maximum energy, collimation, and number properties than FWD protons. In order to confirm this assumption, we measured the BWD and FWD beam divergences for the same shot under HC conditions on a radiochromic film (RCF), using a $13 \mu\text{m}$ thickness target. We repeated the measure covering each time the RCF with a different thickness aluminum foil, in order to record different energy ranges. As shown in Fig. 2 for 2 MeV protons, both beam divergences are indeed found to be identical, with a value at about 4.5° . Moreover, according to the complete set of RCF measures, the total number of accelerated protons with energy greater than 1 MeV for BWD and FWD emission is the same within an error bar about 15% . In summary, BWD and FWD proton bunches show practically the same maximum energy, divergence, and particles number. Indeed, that is completely different from what is usually observed in low contrast experiments [see, for instance, [21]].

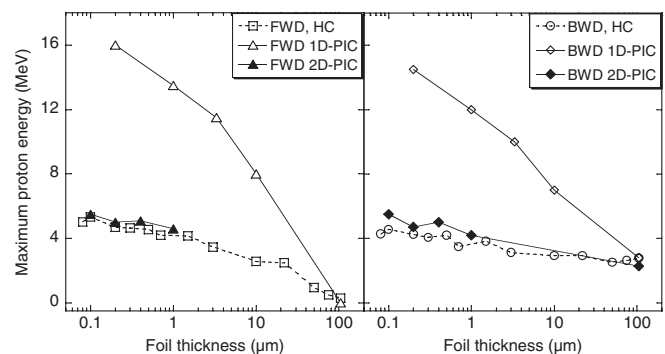


FIG. 3. Comparison of experimental data with numerical predictions for FWD and BWD proton emission of the 1D and 2D PIC simulations.

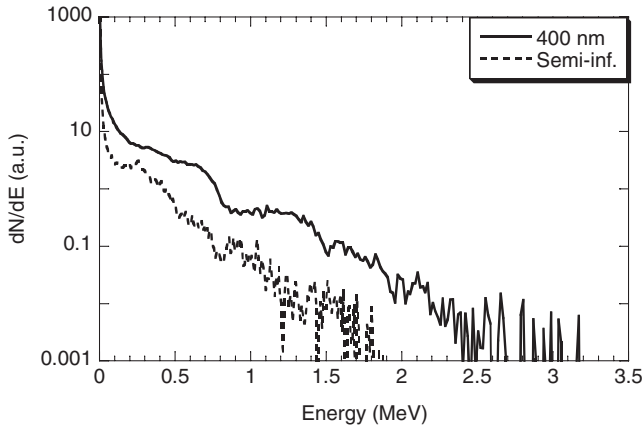


FIG. 4. Electron energy distribution inside the target at the laser peak for a 400 nm and a semi-infinite target.

We compared our experimental results with a series of 1D (EUTERPE [22]) and 2D (CALDER [23]) particle-in-cell simulations accounting for the HC experimental parameters in terms of laser angle of incidence (45°), duration (65 fs), focal spot on the target for the 2D runs ($8 \mu\text{m}$), intensity ($3 \times 10^{18} \text{ W/cm}^2$, slightly lower than the experimental value), and high target density ($150n_c$). In the 1D simulations, oblique incidence is modeled with the “-boosted-frame” technique [24]. These simulations have been run over more than 560 fs, allowing for efficient energy exchange between heated electrons and ions. The computed peak proton energies in the FWD and BWD directions are plotted in Fig. 3.

Missing transverse divergence effects of electrons spreading through the target in the 1D simulation lead to a larger hot electron density and higher proton energy. On the contrary, 2D simulations take correctly into account the electron transport divergence as it is shown by the quite good agreement observed over all the explored thickness range. In 1D simulation, the point at $105 \mu\text{m}$ is obtained setting a semi-infinite target. As a consequence, hot electrons just pass through the target, and ions are no longer accelerated after the laser pulse. Actually, for such a large thickness, electron recirculation [25] tends to vanish and 2D effects become negligible during the short time of acceleration. In this case, the good agreement between

experimental data and 1D simulations prove the value of the description of hot electron generation. FWD and BWD peak ion energies vary similarly both in experiments and simulations, showing a gentle increase with decreasing target thickness. This can be explained by a fast target density decrease and related electron heating enhancement [26] coupled to an effective trapping of the hot electron population around the target. Figure 4 shows the electron spectra at the laser peak for a 400 nm and a semi-infinite target. Reducing the target thickness does increase the electron number as well as their mean and maximum energy. Moreover, the phase space plot of electron and the related spectra of the emitted protons show an evident symmetry as regards the target plane (Fig. 5).

Usually, the dominant heating mechanisms in the small scale length plasmas are essentially the $j \times B$ absorption and the resonance absorption [27]. However, for an oblique laser incidence on a very steep density gradient plasma, we expect that the energy transfer to the hot electron population be a function of the laser polarization [28] through, for instance, the Brunel effect [29] or the mechanism suggested by Gibbon [30] for collisionless absorption of p -polarized short pulses. According to it, the oblique incidence of a p -polarized pulse creates the conditions for an efficient transfer of laser energy to hot electrons. Electrons are pulled back and forth from the target surface by the normal component of the laser electric field and ion restoring force, this creating a mean electric field in front of the target. This field pulls the ions outward and creates a near critical ion shelf in front of the overdense target, the target staying confined by ponderomotive force. As the ion shelf expands over a fraction of wavelength, the restoring force decreases, and the electron oscillations become larger, improving the laser absorption and the hot electron component energy. The Brunel effect as well as the aforesaid dynamics cannot take place effectively for an s -polarized pulse or at normal incidence, where electrons are not dragged *across* but *inside* the target surface. We experimentally checked the effective influence of the laser polarization on the maximum proton energy by inserting a zero-order half wave plate on the beam path. Data obtained for a $13 \mu\text{m}$ Mylar target are presented in Fig. 6. For both FWD and BWD emissions, proton energies continuously

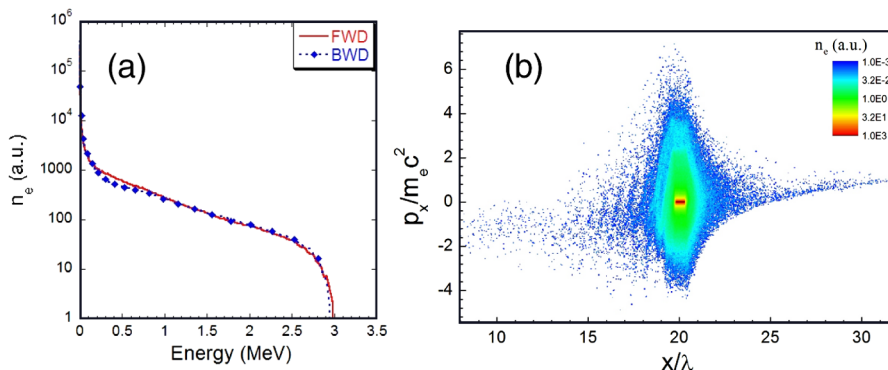


FIG. 5 (color online). (a) Proton energy distribution in the FWD and BWD direction for a 400 nm target and (b) related electron phase space plot at the laser peak.

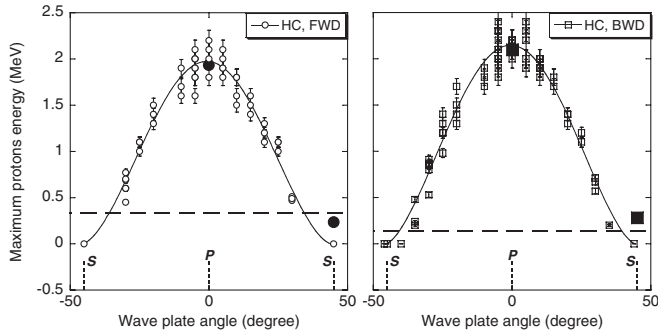


FIG. 6. Plot of maximum proton energy as a function of the laser polarization in the HC case in the FWD (left) and BWD (right) direction. The laser p (s) polarization corresponds to the 0° (45°) wave plate angle. The solid line is the best fit using the function defined in the text. The horizontal dashed lines show the detection thresholds for FWD (0.33 MeV) and BWD (0.14 MeV) emissions. The full symbols represent the points obtained from 2D PIC simulations, normalized to the experimental mean values for p polarization.

decrease when the laser polarization is varied from p (0° wave plate angle) to s (45° angle), and for an s -polarized electric field, the signal completely vanishes. The data have been remarkably well fitted using a simple power scaling of the form $E_{\text{pmax}} \propto \{[\cos(2\vartheta)]^2\}^a$ where ϑ is the wave plate angle and $a \cong 0.8$ for both emissions. We have performed additional 2D PIC simulations changing to s the polarization of the beam impinging on a 400 nm target (a 3D code should be needed to correctly reproduce the effects of intermediate polarization values). A lower laser intensity (about 1.5×10^{18} W/cm 2) has been used in order to take care of the enlarged spot size and loss of laser energy due to the introduction of the 40 mm diameter half-wave-plate (the top-hat laser beam spatial profile diameter being about 60 mm). The p to s maximum proton energy variation given by simulations is in close agreement with experimental points as reported on Fig. 6. The comparison with data obtained under very similar conditions but at lower laser contrast [28] clearly points out the deeper insight in energy transfer mechanisms allowed by very high contrast pulses. As a matter of fact, when we repeated this measurement under LC conditions, the peak proton energy for the s -polarized pulse was found to be only 35% weaker than for a p -polarized pulse, in quite good agreement with [28]. This striking result clearly implies and, to our knowledge, is the first experimental proof that for short and high contrast laser pulses with intensities lying about 10^{18} W/cm 2 , the hot electron and proton energies are actually mostly related to the p -component of the laser electric field rather than to the ponderomotive potential.

In conclusion, thanks to an ultrahigh-contrast laser (10^{10}) and ultrahigh-intensity pulses ($>10^{18}$ W/cm 2), we clearly show that proton energy increases with decreasing target thickness and that the TNSA concept applies for both target surfaces. In addition, we demonstrate that, under these interaction conditions, the proton's acceleration is essentially related to the p -component of the laser electric field. We demonstrate also that it is possible to efficaciously accelerate protons even with very short (65 fs) pulses. The contrast of laser pulses is therefore a key issue for interaction experiments to be used as benchmarks for theories and models.

The authors would like to acknowledge fruitful discussions with Dr. P. Mora (CPhT, France) and Dr. P. Audebert (LULI, France). The allocation of computing resources from the Centre de Calcul Recherche et Technologie (Bruyères-le-Châtel, France) Commission is acknowledged. This work was partly supported by the Conseil Général de l'Essonne (ASTRE program).

- [1] E. L. Clark *et al.*, Phys. Rev. Lett. **84**, 670 (2000).
- [2] R. A. Snavely *et al.*, Phys. Rev. Lett. **85**, 2945 (2000).
- [3] S. P. Hatchett *et al.*, Phys. Plasmas **7**, 2076 (2000).
- [4] M. Borghesi *et al.*, Phys. Rev. Lett. **94**, 195003 (2005).
- [5] K. W. D. Ledingham *et al.*, Science **300**, 1107 (2003).
- [6] M. Tabak *et al.*, Phys. Plasmas **1**, 1626 (1994).
- [7] T. E. Cowan *et al.*, Phys. Rev. Lett. **92**, 204801 (2004).
- [8] M. Borghesi *et al.*, Phys. Rev. Lett. **92**, 055003 (2004).
- [9] A. Maksimchuk *et al.*, Phys. Rev. Lett. **84**, 4108 (2000).
- [10] P. McKenna *et al.*, Phys. Rev. E **70**, 036405 (2004).
- [11] S. C. Wilks *et al.*, Phys. Plasmas **8**, 542 (2001).
- [12] J. Fuchs *et al.*, Phys. Rev. Lett. **94**, 045004 (2005).
- [13] D. Neely *et al.*, Appl. Phys. Lett. **89**, 021502 (2006).
- [14] A. Lévy *et al.*, Opt. Lett. **32**, 310 (2007).
- [15] H. C. Kapteyn *et al.*, Opt. Lett. **16**, 490- (1991).
- [16] H. Schwöerer *et al.*, Nature (London) **439**, 445 (2006).
- [17] S. Ter-Avetisyan *et al.*, J. Phys. D: Appl. Phys. **38**, 863 (2005).
- [18] M. Kaluza *et al.*, Phys. Rev. Lett. **93**, 045003 (2004).
- [19] I. Spencer *et al.*, Phys. Rev. E **67**, 046402 (2003).
- [20] T. Nayuki *et al.*, J. Appl. Phys. **100**, 043111 (2006).
- [21] T. Fujii *et al.*, Appl. Phys. Lett. **83**, 1524 (2003).
- [22] E. Lefebvre and G. Bonnaud, Phys. Rev. E **55**, 1011 (1997).
- [23] E. Lefebvre *et al.*, Nucl. Fusion **43**, 629 (2003).
- [24] P. Gibbon and A. R. Bell, Phys. Rev. Lett. **68**, 1535 (1992).
- [25] A. J. MacKinnon *et al.*, Phys. Rev. Lett. **88**, 215006 (2002).
- [26] P. Antici *et al.*, Phys. Plasmas **14**, 030701 (2007).
- [27] M. I. Santala *et al.*, Phys. Rev. Lett. **84**, 1459 (2000).
- [28] A. Fukumi *et al.*, Phys. Plasmas **12**, 100701 (2005).
- [29] F. Brunel, Phys. Rev. Lett. **59**, 52 (1987).
- [30] P. Gibbon, Phys. Rev. Lett. **73**, 664 (1994).